FOREX Publication
Open Access | Rapid and quality publishing

International Journal of
Electrical and Electronics Research (IJEER)
Research Article | Volume 12, Issue 1 | Pages 99-110 | e-ISSN: 2347-470X

Optimizing Current Injection Technique for Enhancing Resistivity Method

Sifa Nurpadillah[1], Willy Anugrah Cahyadi[2], Husneni Mukhtar[3]*, Kusnahadi Susanto[4], Akhmad Fauzi Ikhsan[5] and Agung Ihwan Nurdin[6]

[1,5,6]*Department of Electrical Engineering, Universitas Garut, Indonesia*
[2,3]*School of Electrical Engineering, Telkom University, Indonesia*
[4]*Department of Geophysics, Faculty of Mathematics and Natural Sciences, Padjadjaran University, Indonesia*

***Correspondence:** husnenimukhtar@telkomuniversity.ac.id

ABSTRACT- Geo-electrical resistivity methods are widely used in various fields and have significant applications in scientific and practical research. Despite the widespread use of resistivity methods, current injection is a critical step in the process of resistivity methods, and the quality of current injection significantly impacts the accuracy of the resistivity measurements. One primary challenge is optimizing current injection techniques to enhance resistivity methods. The developed current injector model for the resistivity meter instrument enhances performance by increasing the voltage source to 400 Volts, extending measurement coverage. It provides three injection current options, 0.5A, 0.8A, and 1A, for efficient accumulator use, considering electrode distances and estimating earth resistance using Contact Resistance Measurement (CRM) to estimate the earth resistance. CRM mode ensures proper electrode connection before injection, thus improving measurement efficiency. The embedded TTGO LoRa ESP32 SX1276 facilitates wireless communication over 1.5 km, addressing challenges in remote and internet-limited areas. The model demonstrates reliability, validity, and durability in CRM mode and current injection measurement. Regarding reliability, we determine the relative error of the model by carrying out measurements repeatedly. In lab-scale testing, the average Relative Error in CRM mode is 0.65%, and in earth resistance measurement testing, it is 1.58%. These relative errors are below the 2% maximum error applied in the "Supersting", a commercial resistivity instrument. The model's validity is defined by comparing the model with the measuring instrument; we have absolute error. In lab scale testing, the average Absolute Error in CRM mode is 3.08%, and in earth resistance measurement testing, it is 3.73%. The model's durability is tested by injecting current for a minute. After one minute of current injection, the power resistor component's temperature is stable at 30°C.

Keywords: Current injector; geo-electrical; contact resistance measurement; resistivity

ARTICLE INFORMATION

Author(s): Sifa Nurpadillah, Willy Anugrah Cahyadi, Husneni Mukhtar, Kusnahadi Susanto, Akhmad Fauzi Ikhsan and Agung Ihwan Nurdin;

Received: 08/11/2023; **Accepted**: 20/01/2024; **Published**: 05/02/2024;
e-ISSN: 2347-470X;
Paper Id: IJEER 0811-07;
Citation: 10.37391/IJEER.120115
Webpage-link:
https://ijeer.forexjournal.co.in/archive/volume-12/ijeer-120115.html

Publisher's Note: FOREX Publication stays neutral with regard to Jurisdictional claims in Published maps and institutional affiliations.

1. INTRODUCTION

Resistivity geo-electrical methods are crucial techniques in understanding subsurface geological characteristics. These methods study the electrical properties below the surface and how to detect them on the surface [1]. In this method, the electrical resistivity of subsurface materials is measured by injecting electrical current into the ground through two current electrodes and measuring the potential difference through two potential electrodes on the surface. The measurement results, namely current and potential differences, produce the resistivity values of each layer beneath the measurement point [2]. The resistivity methods are widely used in various fields and have significant application in both scientific research [3–12] and practical application, for example, in agriculture [13], [14], environmental and geotechnical [15–21], gas exploration [22], geological survey [23–25], and hydrogeology [26–29] field.

Despite the widespread use of resistivity geo-electrical methods, several challenges need to be addressed in those methods. One of the challenges in the resistivity method is current injection. Current injection is a critical step in the resistivity methods process, and the quality of current injection significantly impacts the accuracy of the resistivity measurements. So, we need to address the current injection to enhance the accuracy and efficiency of the resistivity geo-electrical method. Some research about current injection in resistivity meters has been conducted. Making a power supply as a current source with an AC voltage source converted to 12 V DC, a single injection current value, and testing carried out on a lab scale [30]. Designed a resistivity meter with constant current using a boost converter DC-DC, and the test was carried out on a lab scale by loading a resistor [31]. The geoelectric resistivity measurement system uses a constant current source, a boost converter DC-DC with open circuit voltage 250 VDC. There are two current injection options, 0,1 mA and one mA, using a four-point probe as measurement configuration and testing on a lab scale by measuring the resistance of the resistor [32].

FOREX Publication
Open Access | Rapid and quality publishing
International Journal of Electrical and Electronics Research (IJEER)
Research Article | Volume 12, Issue 1 | Pages 99-110 | e-ISSN: 2347-470X

Current injection testing in previous research [30–32] is conducted on a lab scale by measuring the resistance of the resistor. Meanwhile, the current injector on the resistivity meter is practically used in the field by injecting current into the ground directly. There are no variations in the selection of injection current in [30,31]. Meanwhile, variations in injection current in a current injector are needed to determine the amount of power needed to inject current according to conditions in the field. These conditions include the distance between electrodes and subsurface resistance. In research [32], there were two current injection selections. However, the current selection is carried out only by considering the measurement configuration in the field and without considering subsurface resistance. So, the use of power when injecting current is not effective enough. Then, in studies [30–32], the output power from the current injector was insufficient. So, the coverage measurement is limited and not deep enough.

Some of the primary challenges to be addressed are optimizing current injection techniques that can generate more accurate and reliable resistivity data, optimizing current injection to enable the use of resistivity methods in more profound and more relevant applications, considering the integration of modern technology to process resistivity data and enhance data acquisition speed efficiently. Optimizing the current injection on the resistivity meter is carried out by increasing the voltage source during open circuit up to 400 volts, which can increase measurement coverage, adding a contact resistance measurement mode whose results can be used to consider choosing the best injection current value, testing of the current injection is carried out on a lab scale and in the field also so that it can generate more accurate data, and the current injector is given the ability to communicate wirelessly by embedding a TTGO LoRa ESP32 SX1276 microcontroller so that in the future it can be integrated with modern technology. Thus, this research has the potential to advance the field of resistivity methods and significantly contribute to understanding and exploring subsurface resources.

2. MATERIALS AND METHODS

This research develops a higher voltage source of 400 Volts to optimize the design of the "Current Injector Model", which will be used in resistivity meter instruments so that it can increase the coverage of geoelectric meter resistivity measurements with a broader range in the field and the datum points obtained will also be wider and deeper to obtain a subsurface resistivity profile. An accumulator with a specific battery capacity as a power supply was chosen because resistivity meter measurements are often far from residential areas. In addition, this model uses the Contact Resistance Measurement (CRM) mode to estimate earth resistance so that resistivity measurements will be more effective.

The injection model design used three choices of injection current values based on power injection. The operator's choice of injection current value is based on consideration of the distance of the current electrode because earth resistance affects the effectiveness of current injection in the field. Therefore, this model uses Contact Resistance Measurement (CRM) to estimate the earth's resistance and then apply current to the ground after this mode ensures whether the current electrode is connected adequately below the ground surface. Thus, CRM mode provides excess effectiveness in measurement.

A TTGO LoRa ESP32 SX1276 type microcontroller is used so that the electrodes on the resistivity meter can communicate with each other wirelessly such as Bluetooth, WiFi, and LoRa Technology Communication because the measurement field is up to 1.5 km away and the location is in a rural area where no internet network is available. *Table 1* shows the components used in more detail. Component selection is adjusted to system conditions, providing an output voltage of up to 400 volts. These components must be able to work at that voltage.

Table 1: Component selection and Specification

No	Component	Specification
1	LoRa32 V1.0	MCU ESP32, LoRa Chip SX1276, 915 MHz Frequency
2	IPS-DTD12S4001.87 Boost Converter	12VDC to 400VDC, Continuous current 1.5A Power: Peak 750W, continuous 600W
3	LCD12864	Display 128 x 64 Dots Graphic LCD, Type Chip on Board
4	INA219	0 to 26 V Bus Voltages, Max. current 3.2A, Reports current, voltages, and power with 0.5% accuracy
5	SSR-DD	Input control 3-32VDC, Output Control 5A and 400VDC
6	WCS1800	Output voltage AC and DC current, Range 0-35A at 5V, Low operating current 3mA, Isolation voltage 4000V
7	Wire wound Resistor	High power resistor, 100 W for each Resistor

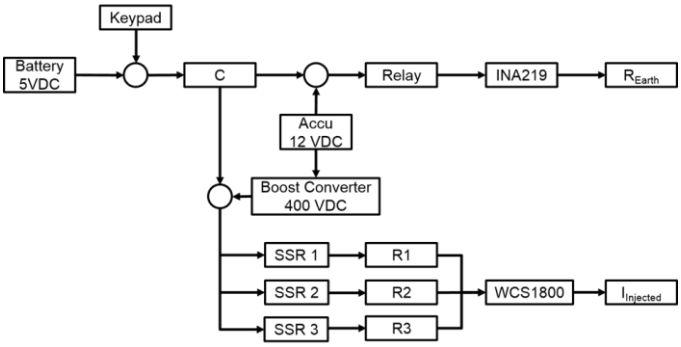

Figure 1: Simulation Diagram of the current injector model

The simulation diagram in *figure 1* shows how the workflow of the model has two modes: CRM measurement to estimate earth resistance and current injection into the earth mode based on the power injection option. The voltage source in CRM mode comes from a 12 V accumulator. The INA219 sensor measures V and I and estimates the earth resistance between the current electrodes. In current injection mode, the voltage source comes from the output of the 400VDC boost converter. The injection power selection is done according to the selected SSR activation

FOREX Publication
Open Access | Rapid and quality publishing
International Journal of Electrical and Electronics Research (IJEER)
Research Article | Volume 12, Issue 1 | Pages 99-110 | e-ISSN: 2347-470X

with a specific injection power. When a current with a certain injection power is injected, the WCS1800 sensor will read the current flowing to the ground.

The design of the current injector model and the Current Injector Model are shown in *figure 2(a)* and *figure 2(b)*, respectively.

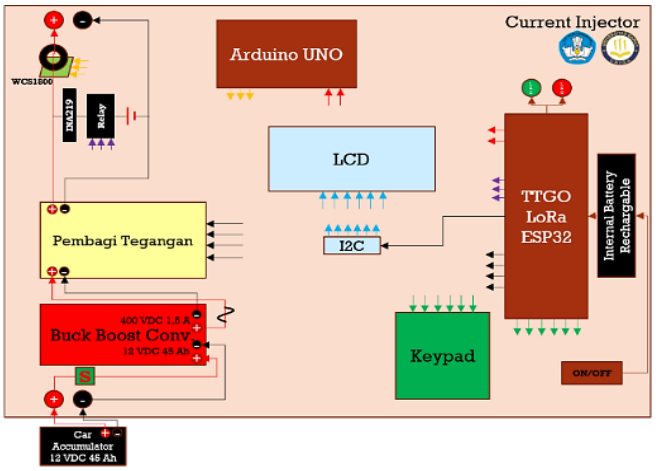

(a)

(b)

Figure 2: The current injector is in the form of (**a**) Model design and (**b**) implemented design

In the Current Injector Model, a boost converter is needed to increase the power supply (dry battery) from 12 Volts to 400 Volts. Then, the output voltage is connected to a voltage divider circuit to produce a selection of injection current according to field needs. The current Injector Model can measure the contact resistance value of the subsurface through the CRM menu. So, the operator can determine the current value to be injected into the subsurface by considering the results of the CRM value and the measurement configuration in the field. Then, the model will inject the selected current. Controlling of the model is carried out by the ESP32 microcontroller by activating the four existing relays. Suppose the CRM test is okay, and the current selection has been determined. In that case, the selected relay will be "ON," and a current value that has been chosen immediately flows from the boost converter to the current electrode, which is plugged into the subsurface.

The flowchart of this current injector model is shown in *figure 3*. The process starts with placing the current electrodes on the surface and wiring them to the injector. After all the equipment is installed, the model will measure contact resistance via the "CRM" menu displayed on the screen. The selection is made using the keypad as the human interface. On the “CRM’ mode, the relay connected to the INA219 sensor is ON. We have a closed loop circuit here, source 12 V from the accumulator and earth as load. Then, INA219 senses the injected current and measures the voltage between electrodes. TTGO LoRa ESP32 calculates the earth resistance using that data. We measure the data 100 times; then, we display the average of earth resistance ($\bar{R}$) and relative error (%E) on LCD. If the CRM results are not OK, we have a caution “Check Connection” on the LCD. If the CRM results are OK, we select the current injection in the resistivity meter. So here we have the current injector model, which informs us whether the model is ready to take measurements. The operators consider CRM results to determine the current value to be injected. In this model, there are three injection current options, namely 0.5A, 0.8A, and 1A. After selecting the injection current, the relay, which is connected to a particular voltage divider circuit, is ON. We have another closed loop here, source 400 volts from Boost Converter and earth as load. The model will be able to inject current into the subsurface automatically. The WCS1800 sensor senses the current and is injected into the ground 100 times. The microcontroller calculates the current average and relative error. That data is displayed on the screen and stored on the memory card.

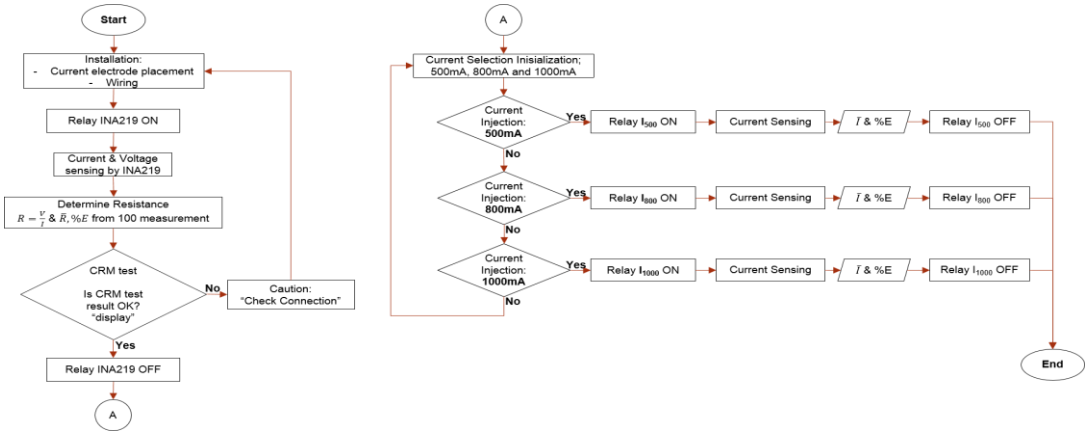

Figure 3: Flowchart of current injector model

FOREX Publication
Open Access | Rapid and quality publishing
International Journal of Electrical and Electronics Research (IJEER)
Research Article | Volume 12, Issue 1 | Pages 99-110 | e-ISSN: 2347-470X

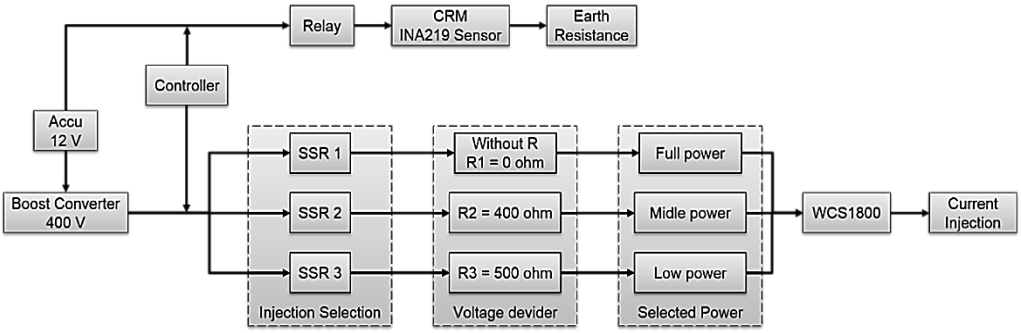

Figure 4: The control diagram of the current injector

The control system of the current injection, in *figure 4*, is used to enhance the resistivity method. It starts with the primary power source from a 12V DC accumulator, which is then converted to 400V DC via a boost converter. The converted voltage is then used as input for the voltage divider circuit, which functions as a current injection selector and relates to power injection. This circuit consists of power resistors arranged in series (as shown in *figure 5*) and controlled by a Solid-State Relay (SSR) connected to a microcontroller TTGO LoRa ESP32 SX1276. As a controller in the system, the microcontroller receives a command from the keypad to select the modes, either the CRM or the injection current. The CRM relay is activated by selecting the CRM menu, and the 12VDC powers the circuit from the accumulator. The system also has an INA219 sensor, which reads voltage and current on the CRM mode circuit. It provides voltage and current data to the microcontroller to estimate earth resistance.

The estimated earth resistance is used to consider power injection selection in the current mode, which has three power injection selections (low, middle, and full power) powered by 400 VDC and activated by certain SSRs. The output voltage depends on earth resistance, up to 400VDC. The WCS1800 sensor is also equipped with the current injector mode. When a certain SSR is activated, the current is injected into the ground with a particular power injection. The WCS1800 sensor measures the injected current and provides current data to the microcontroller. The results of estimated earth resistance measurements by CRM menu and injecting current by current injection menu are displayed on LCD. The appropriate injection current is selected according to field requirements, such as the distance of current electrodes and estimated earth resistance by the CRM menu. Thus, this system provides efficiency in current injection by considering the measured estimated earth resistance, allowing the operator to make a more precise choice of injection current according to field conditions.

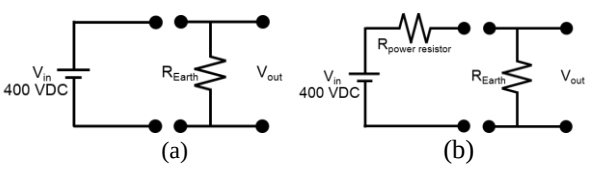

Figure 5: The circuit schematic of injecting current to the ground/ the earth is (a) directly connected to the 400VDC Boost Converter and (b) to a particular power resistor

When injecting current to the ground, output voltage depends on the activated SSR and the earth resistance. Based on the datasheet, the boost converter has an output voltage of 400 VDC and 1.5 A constant current. If the current electrodes plugged into the ground are connected directly to the output of the boost converter (as in *figure 5 (a)*), then a full injection power of 600 Watts is achieved, and the voltage output between the current electrodes, Vout, is maximum and equal to boost converter voltage of 400V. Meanwhile, when the current electrodes plugged into the ground are connected to the power resistor on the divider circuit (shown in *figure 5 (b)*), we have a power resistor ($R_{power\ resistor}$) connected to the earth (R_{Earth}) in series through current electrodes. The same current flows in both circuits. Applying Ohm's Law to each resistor, we obtain:

$$V_{power\ resistor} = iR_{power\ resistor},\ V_{out} = iR_{Earth} \quad (1)$$

$$I = \frac{V_{in}}{R_{power\ resistor}+R_{Earth}} \quad (2)$$

$$V_{out} = V_{in}\frac{R_{Earth}}{R_{power\ resistor}+R_{Earth}} \quad (3)$$

In equation 3, the voltage at the current electrodes, V_{out}, depends on the earth's resistance, R_{Earth}. V_{out} varies according to the earth's resistance. The higher the earth resistance, the closer the output voltage (V_{out}) to the boost converter's input voltage (V_{in}), which is 400V.

3. RESULTS

Testing was conducted on current injection without a dummy resistor to determine the injected current value for each current selection. Once the system is known to be able to inject current with several current options, the next test is carried out. The following tests are testing current injection on a load: laboratory and field scale tests. This current injector model was optimized in terms of adding CRM mode. Therefore, it is necessary to test the model in CRM mode before testing the current injection on a load.

3.1 The Testing of Current Injection Selection

Data collection on the passage of injection current without a dummy resistor was carried out to determine whether the model could inject current as planned, namely 0,5A, 0,8A, and 1A. The test circuit is shown in *figure 6*. We designed three current

FOREX Publication
Open Access | Rapid and quality publishing
International Journal of Electrical and Electronics Research (IJEER)
Research Article | Volume 12, Issue 1 | Pages 99-110 | e-ISSN: 2347-470X

injection selections using a voltage divider circuit and relays as the switching.

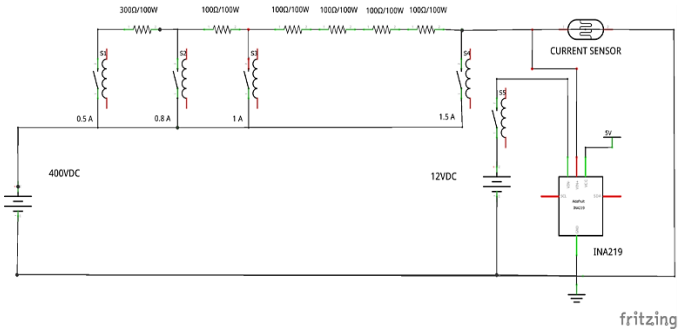

Figure 6: Injection current selection block circuit

Table 2: Data test for current injection selection

No. of iteration	I_{CS1} (A) Relay 1 (R_{PR} = 792 (Ω))	I_{CS2} (A) Relay 2 (R_{PR} = 492 (Ω))	I_{CS3} (A) Relay 3 (R_{PR} = 394 (Ω))
1	0.46	0.72	0.84
2	0.46	0.71	0.84
3	0.46	0.70	0.84
4	0.46	0.70	0.83
5	0.46	0.70	0.83
6	0.46	0.70	0.83
7	0.46	0.70	0.83

R_{PR} (Resistance of power resistor)

Based on *table 2*, the model can inject current with three choices of injection current values. Relay 1 provides an injection current of 0.46A with a relative error of 0%. Relay 2 provides an injection current of 0.70A with a relative error of 1.12%. Relay 3 provides an injection current of 0.83A with a relative error of 0.64%. This test shows that the current injector model can provide three different injection current selections, which refer to different power injections on each selection. However, the third relay current injection significantly differs from the designed current injection selection.

3.2 The testing of CRM mode

We optimize the current injector model by adding CRM mode. This mode provides information on whether the electrode is connected correctly or not. Furthermore, the CRM mode also provides the earth resistance information between the current electrodes. The value obtained can be used as a consideration for the operator to choose an efficient injection current. CRM mode on the current injector model uses INA219, a current and power sensor that gives the total energy consumed by the shunt load and provides output in digital form. It can handle a high current of up to 3.2A and a maximum voltage of up to +26 V [33]. In previous research, the INA219 sensor has been utilized for voltage measurements [34,35], current size [36–43], voltage and current measurement [44]–[54], and for the voltage, current and power consumption [55–60]. We modified the microcontroller program of the INA219 sensor on TTGO LoRa ESP32 to be used to determine the earth's resistance. We calculate the earth resistance below the current electrodes using Ohm's Law with the measured voltage and current using INA219. INA219 sensor reliability testing on a lab and field scale is conducted in the CRM mode. Experimental data (as raw data) for each test is presented in graphics (*figures 7 to 13*). Relative error ($E_{relative\ std}$) relates to variations in measured results, which indicate the consistency of measurements made by the model. At the same time, the absolute error ($E_{absolute}$) is the result of comparing measurements made by the model with commercial instruments.

$E_{(relative\ std)} = (\sigma/N)100$, σ is the standard deviation, and N is the number of measurements.

$E_{absolute} = ((x_i - x_I)/N)100$, x_i is measurement data from the model, x_I is measurement data from commercial instruments as a comparison, and N is the number of measurements.

3.2.1 Lab Scale CRM Mode Testing

In lab scale testing, three different resistors: R1 = 50.91 ohm, R2 = 300.7 ohm, and R3 = 1955 ohm. The 12 Volt DC of the power supply is connected to the resistor. TTGO LoRa ESP32 SX1276 calculated the resistance of the resistor (R1, R2, and R3) by voltage and current measurement from the INA219 sensor. The measurements are carried out repeatedly, 20 times, and the raw data is shown in *figure 7*. It shows the results of resistance measurements in lab scale testing using the INA219 sensor. Laboratory-scale testing determined the average resistances for each resistor through INA219 sensor readings, resulting in values of 51.3 ohms, 295.6 ohms, and 1823.5 ohms for resistors R1, R2, and R3, respectively. The relative errors associated with these resistance measurements are impressively low, with a mere 0.07% for R1, 0.39% for R2, and 1.5% for R3. These minimal relative errors signify high precision and accuracy in our measurements. Notably, the slight variation observed in the Contact Resistance Measurement (CRM) mode further validates the consistency of our measurements.

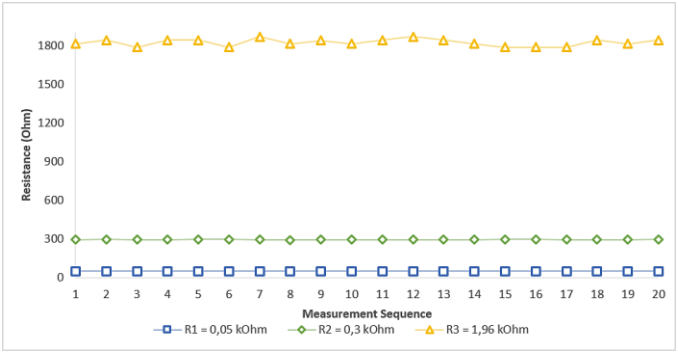

Figure 7: Resistance measurement on CRM mode using INA219

We conducted resistance measurements using the Contact Resistance Measurement (CRM) mode on the model and compared these results with measurements obtained from a multimeter. The Mean Percentage Absolute Error (MAPE) was calculated for each resistance measurement to assess the accuracy of the CRM mode on our current injector model. Remarkably, we observed a low MAPE of 0.79% for R1 (50.91

FOREX Publication
Open Access | Rapid and quality publishing
International Journal of Electrical and Electronics Research (IJEER)
Research Article | Volume 12, Issue 1 | Pages 99-110 | e-ISSN: 2347-470X

ohms), indicating high precision in CRM measurements for this resistor. Similarly, for R2 (300.7 ohms), the MAPE was 1.71%, signifying excellent accuracy compared to multimeter readings. While R3 (1955 ohms) exhibited a slightly higher MAPE of 6.73% it still falls within an acceptable range, showcasing the overall reliability and effectiveness of the CRM mode in our lab-scale testing. These results affirm that the current injector model, particularly in CRM mode, provides highly accurate resistance measurements, demonstrating its robust performance in a controlled laboratory environment.

3.2.2 Field scale CRM mode testing

Contact Resistance Measurement (CRM) mode testing on a field scale was carried out under two distinct soil conditions: *dry and hydrated*. A 12 Volt DC power supply was connected to both ends of the current electrode, with the two electrodes grounded 15 meters apart in the earth. Using the INA219 sensor, we measured the earth resistance between these electrodes. *Figure 8* illustrates the outcomes of earth resistance measurements for dry and hydrated soil conditions. Concerning the consistency of measurement results, we observe that in the field-scale test under both dry and hydrated soil conditions, the average earth resistance obtained using the INA219 sensor was 1109.61 ohms for dry soil and 906.99 ohms for hydrated soil.

Furthermore, the relative errors for each earth resistance measurement were 1.95% for dry soil and 1.22% for hydrated soil. The low relative errors indicate that the current injector model consistently provides precise measurement results, even under varying soil conditions. Moreover, the low variability in CRM mode measurements at the field scale provides additional confidence in the model's consistency. The high consistency in measuring earth resistance illustrates that this model can be relied upon to generate accurate and dependable data in the field, even amidst significant variations in soil conditions. This result underscores the model's effectiveness in geoelectric resistivity measurements across diverse environmental and field conditions.

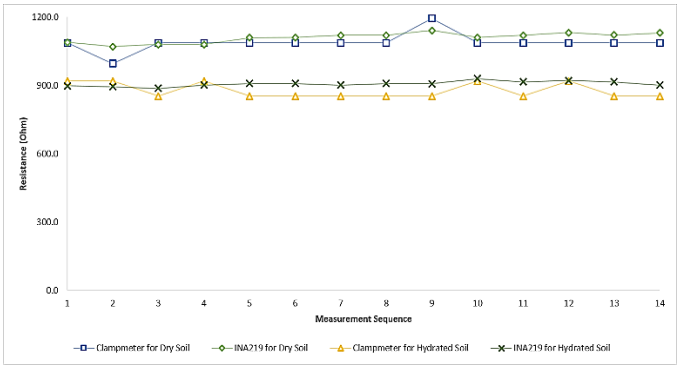

Figure 8. Comparisons of earth resistance measurement using Contact Resistance Measurement mode with INA219 in dry and hydrated soils

A comparison was made between the earth and earth resistances data from CRM mode and the multimeter to analyze the measurement accuracy comprehensively. The Mean Percentage Absolute Error (MAPE) was calculated for each earth resistance measurement under dry and hydrated soil conditions. The results revealed a low MAPE of 2.92% for dry soil conditions and 4.54% for hydrated soil conditions. These low MAPE values signify an impressive level of accuracy in the CRM mode of the current injector model during field-scale testing. The deviation between the CRM mode measurements and multimeter readings is minimal, emphasizing the model's robustness in providing highly accurate earth resistance data. The exemplary accuracy demonstrated under real-world field conditions enhances the credibility and reliability of the current injector model for geoelectric resistivity measurements in diverse soil environments.

3.3 The testing of current injection

We already had a current injector model with three current injection selections with their power injection. Additionally, CRM mode has been added to the current injector model. After the CRM mode provides the measurement results, the operator can determine whether this model can inject the current. Then, the operator considers the amount of current injected into the earth based on the measurement results in CRM mode. After determining the current selection that will be injected into the earth, the relay connected to the selected current selection will be ON. Then, the current flows to the earth through both current electrodes. In this injection process, the model must measure the current loaded by the earth's resistance. Please remember that when injecting the current selected, the source comes from the boost converter output of 400 Volts. Using high voltage DC while injecting current, we need a Hall's effect current sensor to measure the current injected. We have chosen a hall effect ACS712 to measure its current. However, the ACS712 sensor gets ruined. This Hall's Effect sensor is unsuitable for this current injector model and may be due to the direct connection between the ACS712 sensor module and the cable in which the current will be measured. As an alternative, we chose another Hall's Effect current sensor, the WCS1800 sensor, to measure the current. Although this sensor has a more extensive range of current measurements than ACS712, the WCS1800 sensor succeeded in measuring the current.

However, in measuring current with the WCS1800, Arduino Nano has been added as a microcontroller. Then, the measurement results are transferred to TTGO LoRa ESP32. The addition of the Arduino Nano was made because we had yet to find a solution so that the WCS1800 could be compatible with TTGO. The test was conducted to determine the reliability of the WCS1800 sensor on the Current Injector Model that will be used to measure the injected current into the ground. The test consists of lab and field scale tests.

3.3.1 Lab scale injection current testing

In lab scale WCS1800 testing, four resistors with different resistances were used: R1 = 20 ohm, R2 = 50.91 ohm, R3 = 80 ohm, and R4 = 100 ohm. The source, 12 Volt DC from a power supply, is connected to the resistor. We measured the current

FOREX Publication
Open Access | Rapid and quality publishing
International Journal of Electrical and Electronics Research (IJEER)
Research Article | Volume 12, Issue 1 | Pages 99-110 | e-ISSN: 2347-470X

through the resistor by the WCS1800 sensor (*figure 9*). The average currents are obtained from each resistor by the WCS1800 sensor readings, namely 643.7 mA, 246.0 mA, 162.1 mA, and 143,2 mA. The relative errors in each current measurement are 1,11%, 1,80%, 3.18%, and 5.7%. Based on this lab scale test, we obtained that the variation of current size is low for 643.7 mA, 246,0 mA, and 162,1 mA current measurements and moderates for 143.2 mA current measurement. It shows that the variation in measurement results becomes more similar for the more significant the current measurement range. However, as the WCS1800 measures currents in the range of 140mA, the standard variation is moderate. It means the WCS1800 can still be used in some applications. Hence, the measurement consistency is good enough.

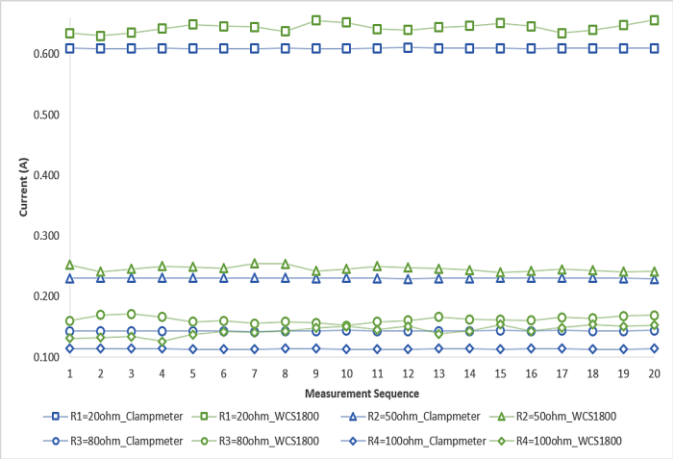

Figure 9: Current measurements by WCS1800 sensor on lab scale measurement for each resistance value (20 ohms, 50.91 ohms, 80 ohms, and 100 ohms) with 12 volts, respectively, yield the average currents of 643.7 mA, 246.0 mA, 162.1 mA, and 143.2 mA

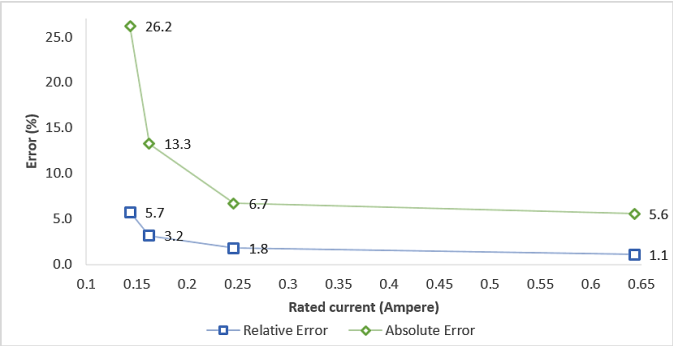

Figure 10: Absolute and relative error on WCS1800 sensor readings in lab scale measurement

Validating the current readings of WCS1800 with a clamp meter, the Mean Percentage Absolute Error (MAPE) was calculated for each current measurement. The specific MAPE values obtained were 5.59% for 643.7 mA current, 6.73% for 246.0 mA current, 13.27% for 162.1 mA current, and 26.16% for 643.7 mA current. The performance of WCS1800 in lab-scale testing indicates a good accuracy for current measurements exceeding 150 mA and acceptable accuracy for current measurements below 150 mA. The lower MAPE values for higher current measurements indicate higher accuracy and precision of WCS1800 readings. However, it is worth noting that the WCS1800 still provides acceptable accuracy even for lower current measurements, demonstrating its reliability across a broad range of current levels. This comprehensive assessment affirms the WCS1800's suitability for accurate, current measurements in diverse laboratory conditions, enhancing its applicability in various scenarios.

The absolute and relative errors of current measurements, as illustrated in *figure 10*, indicate that the WCS1800 sensor has a reliable performance across various current levels, even in higher currents, because its reading is within acceptable limits. The demonstrated reliability of the WCS1800 sensor further validates its suitability for use in various applications, affirming its role as a trustworthy component within the current injector model. One key strategy to enhance accuracy is highlighted: operators can compensate for potential inaccuracies in WCS1800 readings by considering CRM results. This integrated approach allows for a more refined and accurate current measurement process, mainly when dealing with higher current levels.

3.3.2 Field scale injection current testing

Field-scale WCS1800 testing is conducted to determine the reliability and validity of current measurements on the current injector model in the field. Here, we use a direct source from the current injector model, with four different power output options when injecting current, represented by selecting a specific injection current. Using the Current Injector Model, the source is connected to both ends of the current electrode. The two current electrodes are grounded to the earth 20 meters from each other. We measure the current through the planet using the WCS1800 sensor. *Figure 11* shows the results of the current measurement through the earth using the WCS1800 sensor; for current injection selection 0,5 A power injection 139.5W, WCS1800 sensor read average current is 153.9mA; for current injection selection 0.8 A power injection 251.2W, WCS1800 sensor read 151.1mA average current; for current injection selection 1 A power injection 326.4W, 155.9mA average current read by WCS1800; for the last, 204.2mA and 359.4mA are the average current measurement by WCS1800 for total power injection (585.45W) current on dry and hydrated soil condition. The relative errors in each current measurement are 2,58%, 1.95%, 1.95%, 1.36%, and 1.12%. Based on this field scale test, we obtained that the variation of current measurement is low for all injection current selections. It shows that the recent measurement results by WCS1800 on the field scale test provide data measurement with good consistency.

FOREX Publication
Open Access | Rapid and quality publishing
International Journal of Electrical and Electronics Research (IJEER)
Research Article | Volume 12, Issue 1 | Pages 99-110 | e-ISSN: 2347-470X

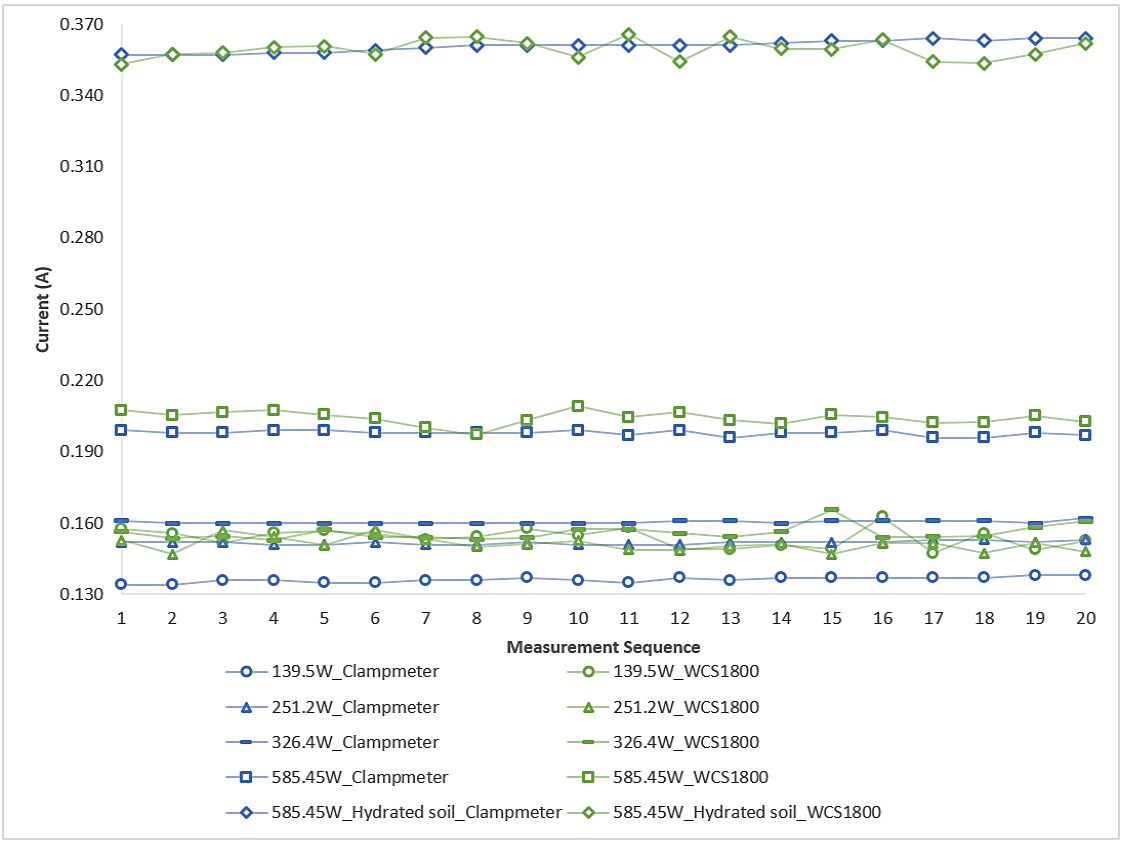

Figure 11: Current measurement by WCS1800 sensor on field scale measurement

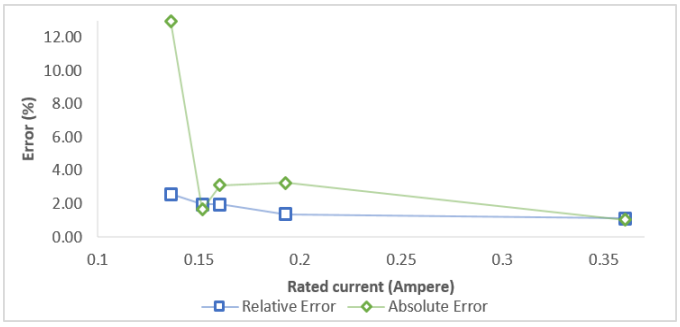

Figure 12: Absolute and relative error on WCS1800 sensor readings in field scale measurement

As shown in *figure 11*, the Mean Percentage Absolute Error (MAPE) values of the sensor and a clamp meter for each current measurement are 12.98% for 153.9 mA, 1.64% for 151.1 mA, 3.12% for 155.9 mA, 3.25% for 204.2 mA, and 1.04% for 359.4 mA. An adequate accuracy was obtained for more significant and current measurements less than 150 mA. The higher MAPE values of lower current measurements (around 150 mA) provide a slightly lower accuracy than higher currents. Nevertheless, the consistently low MAPE values for currents greater than 150 mA indicate that the WCS1800 maintains a good accuracy for higher current levels. This nuanced analysis underscores the reliability of the WCS1800 in capturing current measurements in diverse field conditions. While slightly less accurate in lower current ranges, the model remains sufficiently reliable for practical field applications.

The comparison between absolute error and relative error in current measurements on the field scale test (*figure 12*) demonstrates accuracy in current measurements. It suggests the potential for even greater precision when measuring larger currents. Operators can strategically leverage CRM results to enhance accuracy, compensating for potential inaccuracies in WCS1800 readings. The meticulous comparison of absolute and relative errors and the sensor's consistent performance supports the conclusion that the current injector model, equipped with the WCS1800 sensor, is reliable, valid, and well-suited for accurately measuring injection current in diverse field conditions. These findings contribute to the model's overall robustness and efficacy in practical applications.

3.3.4 The testing of power resistor durability

As previously stated, six power resistors are connected in series in the injection current selection block, as shown in *figure 6*. After testing the current injection (either without a dummy resistor or with a dummy resistor), the temperature of the power resistor is measured. This measurement is conducted to determine the durability of the power resistor components during current injection.

The temperature of the power resistor after injecting current for 1 minute is shown in *figure 13*. The power resistor temperature is highest for the circuit without a dummy resistor. The

FOREX Publication
Open Access | Rapid and quality publishing
International Journal of Electrical and Electronics Research (IJEER)
Research Article | Volume 12, Issue 1 | Pages 99-110 | e-ISSN: 2347-470X

temperature of the power resistor decreases as the dummy resistor value increases and reaches a safe temperature in the range of 30°C. The dummy resistor acts as the earth; then, it will receive current from the current injector. So, when we use the Current Injector Model in the field, which is connected to the earth, this power resistor on the model has good durability for injecting current to the earth with a resistance of more than 1-kilo Ohm. It means we must be careful and consider low CRM results. So, choose the lower selection of the current injection to deal with that condition. Future work uses constant current using transistors for injection current selection. However, selecting components for the constant current will also be challenging.

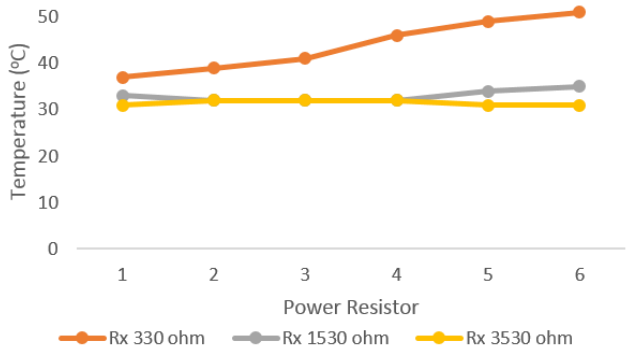

Figure 13: Temperature of power resistor on Current Injector Model after injection. (Rx is a dummy resistor that is connected to the model)

4. DISCUSSION

The principle of geoelectric resistivity meter measurement is injecting electric current into the ground and measuring electric potential distribution using electrodes on the surface. One of the successes of geoelectric measurements depends on the current injection block. In this paper, we optimize the current injection block on the resistivity meter, which consists of several current injection options. The selection of the current to be injected into the earth is according to the CRM results. This optimization was carried out using the TTGO LoRa ESP32 microcontroller.

A voltage divider circuit uses several power resistors and relays to select the injection current. The power resistor was chosen to accommodate high DC voltage sources, up to 400 volts. When one of the relays is activated using control from TTGO, a particular current value will be injected. This current injection model provides several injection current options: 0.46A 167.6 Watts, 0.70A 241.1 Watts, and 0.83A 271.4 Watts.

In CRM mode, before injecting current with a high voltage source (from boost converter output), the current injection model must be able to inform whether the current electrode pair is connected to the ground. In addition, to save on the injection source (accumulator) usage, the injection model must be able to estimate the earth resistance value before injection. It can be overcome by adding CRM mode to the current injection model. So, the current injection model can estimate the earth resistance value before injection. Earth resistance in CRM mode is obtained by modifying the INA219 sensor. The resistance value is determined using Ohm's law based on the voltage and current readings on the INA219 sensor. Based on the test results of the INA219 sensor in CRM mode, the relative error value is 0.65% for lab scale testing using a dummy resistor and 1.58% for earth resistance testing. It shows that the CRM measurement in the current injection model has consistent measurement results with high precision, and this model has good reliability. This model also has a relative error below the maximum error set by the commercial instrument, “Supersting”, 2%. Then, in CRM mode, the determination of the resistance value is compared with the clamp meter measurement results. So, we can determine the absolute error of the resistance measurement in CRM mode. The absolute error obtained was 3.08% for lab scale tests and 3.73% for earth resistance measurement tests. It can be said that determining earth resistance in CRM mode provides accurate values , and the model has good validity. After 1 minute of injecting current into the earth, we measured the temperature of the power resistor in the voltage divider circuit. The measured temperatures are around 30°C. This means the current injection model is durable when used for field exploration.

All these optimizations were carried out using the TTGO LoRa ESP32 microcontroller. The TTGO LoRa ESP32 SX1276 contributes to geoelectric resistivity measurements in the field by providing wireless communication capabilities. Equipped with LoRa, Bluetooth, and WiFi technologies, the LoRa functionality is essential for facilitating long-range, low-power communication between current and voltage electrodes for remote areas lacking internet connectivity. The TTGO LoRa ESP32 SX1276 not only overcomes communication challenges in remote field settings but also allows for real-time monitoring and control of the system from a distance, improving overall field experiment efficiency. Its seamless integration with embedded systems further enables smooth communication with sensors, data processing, and transmission, making it an integral component in optimizing geoelectric resistivity measurements under varying field conditions.

The use of this product can be divided into two main groups: technicians/engineers in systems engineering and field operators who will be using the model. Here is a more detailed explanation for both groups:

(1) *Technicians/engineers in systems engineering*: Target audience: Professionals with in-depth technical knowledge of systems engineering, power electronics, and ground resistivity measurements. Technical depth: Present detailed technical information, including hardware specifications such as relay types, sensors, microcontroller configuration parameters, and the working principles of each component. The control diagram and explanation will cover in-depth technical aspects, such as microcontroller configuration parameters, sensor characteristics, and the concept of injection current generation.

(2) *Field operators/users*: Target audience: Field operators using the system for ground resistivity monitoring activities. Several fields of work may benefit from this model: geothermal exploration, the mining industry, construction and building foundations, water resource

International Journal of Electrical and Electronics Research (IJEER)
Research Article | Volume 12, Issue 1 | Pages 99-110 | e-ISSN: 2347-470X

management, environmental monitoring, and the oil and gas industry.

The current injector model's practical aspects, including cost, portability, and ease of use, are crucial considerations. In terms of cost, this current injector model can reduce production costs when measuring geoelectric resistivity in the field by reducing cables, which are usually used to connect current and voltage electrodes in the field up to 1.5 km. Then, this current injector model has good portability because it can be used in remote areas even if it lacks an internet connection. In terms of ease of use, operators can effectively inject current in the field because the model provides information on whether the electrodes are correctly connected and what the estimated earth resistance is, which is then used as a consideration for the operator to choose the appropriate current injection selection to make the use of the power supply in the field more efficient.

Recommendation for future work: Current injection selection is provided by constant current; enhance the user interface of the model to improve the field operator's experience. Add features that facilitate ease of use, data analysis, and real-time measurement monitoring; expand the performance testing of this model to larger field scales and diverse geological conditions.

5. CONCLUSION

The optimized current injector model for the resistivity meter instrument introduces vital enhancements to improve its overall performance. The model extends measurement coverage by increasing the voltage source to 400 Volts and deepening subsurface datum points. Offering three injection current choices related to power injection, the model ensures efficient use of the accumulator as a power source, with operators considering electrode distances for optimal current injection. Incorporating Contact Resistance Measurement (CRM) allows for estimating earth resistance, contributing to enhanced current injection effectiveness. The model also employs CRM mode to confirm proper electrode connection before injections, ensuring measurement efficiency. Additionally, the embedded TTGO LoRa ESP32 SX1276 microcontroller with Bluetooth, WiFi, and LoRa Technology Communication facilitates wireless communication over electrode distances of up to 1.5 km, addressing challenges in rural areas with no internet connectivity and providing a robust solution for diverse field conditions.

Author Contributions: "Conceptualization, Husneni Mukhtar and Kusnahadi Susanto; methodology, Willy Anugrah Cahyadi, and Sifa Nurpadillah; validation, Sifa Nurpadillah, and Agung Ihwan Nurdin; formal analysis Sifa Nurpadillah; investigation, Husneni Mukhtar and Willy Anugrah Cahyadi; resources, Akhmad Fauzi Ikhsan; data curation, Sifa Nurpadillah and Husneni Mukhtar; writing—Sifa Nurpadillah; supervision, Husneni Mukhtar, Willy Anugrah Cahyadi, and Kusnahadi Susanto. All authors have read and agreed to the published version of the manuscript".

Acknowledgments: We thank Kemdikbudristek Dikti, LLDIKTI Region IV and Garut University for contributing to this research. This research was funded by the Ministry of Education and Culture, Research, Technology and Higher Education with contract number 180/E5/PG.02.00.PL/2023.

Conflicts of Interest: The authors declare no conflict of interest.

REFERENCES

[1] Kirsch, R.; Yaramanci, U. Geoelectrical methods. Groundwater Geophysics. Springer, Berlin, Heidelberg, 2006, ISBN 978-3-540-29383-5.

[2] Rolia, E.; Sutjiningsih, D. Application of geoelectric method for groundwater exploration from surface (A literature study). AIP Conf. Proc., 2018, 1977, p.020018.

[3] Feranie, S; Putri, A.P.W; Handiman, A.K.P; Tohari, A. Recent development in the use of geoelectric resistivity for landslide surveys: an overview, Gravity J., 2023, 9, p. 130-143.

[4] Yohandri, M; Akmam, Development of a Digital Resistivity Meter Based on Microcontroller. TENCON IEEE Region 10 Conference, 2018, pp. 0551-0554.

[5] Adler, J.; Ginting, S. L. B.; Abdullah, A. R. A.; Akhbar, A. The Design of Resistivity Tool for Subsurface Based on Microcontroller. IOP Conf. Ser.: Mater. Sci. Eng., 2018, 407, p012123.

[6] Widodo, W; Lapanporo, B. P.; Jumarang, M. I. Rancang Bangun Alat Geolistrik Berbasis Arduino Mega2560. Phys. Commun., 2018, 2, pp. 52–62.

[7] Huda, F; Harmadi, H; Pohan, A. F. Prototipe Rancang Bangun Alat Geolistrik Menggunakan Arduino Uno R3 dan Transceiver nRF24L01+. J. Fis. Unand, 2021, 10, pp. 435–444.

[8] Irianto, E. A. Rancang bangun Resistivity Meter Digital dengan Metode Four Point Probe untuk Menentukan Hambatan Jenis Tanah. Jurnal Fisika, 2014, 3, pp. 96–99.

[9] Kutbay, U; Hardalaç, F. Development of a multiprobe electrical resistivity tomography prototype system and robust underground clustering. Expert Syst., 2017, 34, p12206.

[10] de la Vega, M.; Bongiovanni, M. V. et.al. Design of a Low-Cost Electrical Resistivity Meter for Near Surface Surveys," Earth Sp., 2021, 8.

[11] únior, A. O. C.; Pontes-Neto C. F. Design and construction of an automated and programmable resistivity meter for shallow subsurface investigation. Methods Data J., 2022,

[12] Fatahillah, D; Nuryani, N. Low-cost multi electrode resistivity meter based on microcontroller for electric resistivity tomography purpose. J. Phys. Conf., 2019, 1153, pp. 1742-6596.

[13] Ivansyah, O; Nurhasanah, N; Saniah, S. Disain Perangkat Geolistrik Untuk Kegiatan Geofisika Pertanian (Aplikasi Pada Lahan Gambut Kalimantan Barat). SEMIRATA, 2015, pp. 326–355.

[14] Lu, D. Imaging and characterization of the preferential flow process in agricultural land by using electrical resistivity tomography and dual-porosity model. Ecol. Indic., 2022, 134, p. 108498.

[15] Prasetia, A. M; Aidil, R; Faizal, R. Penggunaan Resistivity Meter Berbasis Boost converter Untuk Identifikasi Batuan Dasar Pancang Pondasi Bangunan di Pulau Tarakan. Borneo Eng. J., 2018, 2, pp. 127-136.

[16] Radzicki, K; Gołębiowski, T; Ćwiklik, M; Stoliński, M. A new levee control system based on geotechnical and geophysical surveys including active thermal sensing: A case study from Poland. Eng. Geol., 2021, 293, 106316.

[17] Elkafrawy, S. B; Fattah, T. A; Naiel, T; et.al. Environmental and site characterization investigations using remote sensing and geophysical techniques-a case from Nabq, Gulf of Aqaba, Sinai, Egypt. Remote Sensing Applications: Society and Environment, 2021, 24, 100653.

[18] Raji, W. O; Adedoyin, A. D. Dam safety assessment using 2D electrical resistivity geophysical survey and geological mapping. J. King Saud Univ., 2020, 32, pp. 1123-1129.

[19] Martin, T. Geophysical Exploration of a Historical Stamp Mill Dump for the Volume Estimation of Valuable Residues. J. Environ. Eng. Geophys., 2020, 25, pp. 275–286.

[20] Harja, A.; Ma'arif M, F. R.; Nanda, M. D.; Duvanovsky, D. A.; Tangke, R.; Susanto, K. Studi Hidrogeofisika Gunung Malabar Sebagai Gunung Tertinggi pada Sistem Hidrologi Cekungan Bandung. Jurnal Geologi Dan Sumberdaya Mineral, 2021, 22, 223.

[21] Rahmani, T. R. Using the Schlumberger configuration resistivity geoelectric method to analyze the characteristics of slip surface at Solok. Journal of Physics: Conference Series, 2020, 1481, 102030.

[22] Zhang, P.; Binyang, S. U. N.; Yuan, H. et.al. Artificial intelligence detection system for deep-buried fuel gas pipeline leakage. US Pat. App. 16, 2021.

[23] Pardo-Igúzquiza, E.; Dowd, P. A; Ruiz-Constán, A. et.al. Epikarst mapping by remote sensing. Catena J., 2018, 165, pp. 1-11.

[24] Raji W. O.; Bale, R. B. 2D electrical resistivity imaging of tantalite-bearing veins in Kaiama, Nigeria. NRIAG J. Astron. Geophys., 2022, 11, pp. 306-312.

[25] Conaway, C. H. Permafrost Mapping with Electrical Resistivity Tomography: A Case Study in Two Wetland Systems in Interior Alaska. J. Environ. Eng. Geophys., 2020, 25, pp. 199–209.

[26] Tjiongnotoputera, K. D. Analytical comparison of electrode configuration on 2D geoelectric method for identification of water seepage in the lake body," Journal of Physics: Conference Series, 2021, 1825.

[27] Raji, W.O. Evaluation of groundwater potential of bedrock aquifers in Geological Sheet 223 Ilorin, Nigeria, using geo-electric sounding. Appl. Water Sci., 2020, 10, 1007.

[28] Rey, J.; Martínez, J.; Mendoza, R.; Sandoval, S.; Tarasov, V.; Kaminsky, A.; Hidalgo, M.C.; Morales, K. Geophysical Characterization of Aquifers in Southeast Spain Using ERT, TDEM, and Vertical Seismic Reflection. Appl. Sci. 2020, 10, 7365.

[29] Youssef, M. A. S. Geoelectrical analysis for evaluating the groundwater characteristics of wadi El Madamud Area, Southeast Luxor, Egypt. J. Taibah Univ. Sci., 2020, 14, pp. 1514–1526.

[30] Nayel, M.; Lu, B.; Tian, Y; Zhao, Y. Study of Soil Resistivity Measurements in Vertical Two-Layer Soil Model. Asia-Pacific Power and Energy Engineering Conference, APPEEC, 2012, 6307337.

[31] Susanto, K; Azzam, M. Z; Syarafina, Z. N; Kirana, K. H; Dharmawan, I. A; Harja, A. Investigasi Lapisan Batuan Kawasan Pendidikan Universitas Padjadjaran Jatinangor Bagian Utara Berdasarkan Electrical Resistivity Tomography (ERT). Bulletin of Scientific Contribution: Geology, 2023, 21, pp. 61–70.

[32] Indarto, B; Sudenasahag, G. R. E; Rahmad, D. B. Rancang Bangun Sistem Pengukuran Resistivitas Geolistrik dengan menggunakan Sumber Arus Konstan," Jurnal Fisika dan Aplikasinya, 2016, 12, pp. 83-89.

[33] Malik, P; Gehlot, A; Singh, R; Gupta, L. R. A review on ANN based model for solar radiation and wind speed prediction with real-time data. Computational Methods in Engineering, 2022, 29, p.3183

[34] Pradhan, N.R; Singh, A.; Verma, S. A blockchain-based lightweight peer-to-peer energy trading framework for secured high throughput micro-transactions," Sci Rep, 2022, 12, 14523.

[35] Hamdani, H; Pulungan, A. B; D. E. Myori. Real Time Monitoring System on Solar Panel Orientation Control Using Visual Basic. Journal of Applied Engineering and Technological Science, 2021. 2, pp 112-124.

[36] Lange, E. O; Jose, J. M; Benedict, S; Gerndt, M. Automated Energy Modeling Framework for Microcontroller-based Edge Computing Nodes. Communications in Computer and Information Science, 2022. pp. 422–437.

[37] M. H. Qahtan, E. A. Mohammed, and A. J. Ali, "IoT-based electrical vehicle's energy management and monitoring system," Open Access Library Journal. 2022. pp. 1-15.

[38] Shahid, T; Gouwanda, D; Nurzaman, S. G. Development of an electrooculogram-activated wearable soft hand exoskeleton," 2020 IEEE-EMBS Conference on Biomedical Engineering and Sciences (IECBES), Langkawi Island, Malaysia, 2021. pp. 433-438.

[39] Helal, A. A; Villaça, R. S; Santos, C. A. S. An integrated solution of software and hardware for environmental monitoring. Internet of Things, 2022, 19, p.100518.

[40] Jooss, Y; Rønning, E. B; Hearst, R. J; Bracchi, T. Influence of position and wind direction on the performance of a roof mounted vertical axis wind turbine, Journal of Wind Engineering, 2022, 230, p.105177.

[41] Kang, M; Joe, S; An, T; Jang, H; Kim, B. A novel robotic colonoscopy system integrating feeding and steering mechanisms with self-propelled paddling locomotion: A pilot study," Mechatronics, 2021, 73.

[42] Schultz, J. T; Beck, H. K; Haagensen, T. Using a biologically mimicking climbing robot to explore the performance landscape of climbing in lizards. Proc Biol Sci, 2021, 288.

[43] Cramer, B; Billaudelle, S; Kanya, S. Surrogate gradients for analog neuromorphic computing. Computer Sciences, 2022, 119, p. 833-845.

[44] Pratama, E. G; Sunanda, W; Gusa, R. F. A floating photovoltaic system for fishery aeration. IOP Conf. Ser. Earth Environ Sci, 2021, 926, pp. 1-5.

[45] Le, A. D; Pham, D. A; Pham, D. T; Vo, H. B. Alert Trap: A study on object detection in remote insects trap monitoring system using on-the-edge deep learning platform. Published in arXiv.org, 2021, pp. 1-15.

[46] Jang, Y. W. et al. Intact 2D/3D halide junction perovskite solar cells via solid-phase in-plane growth. Nat. Energy, 2021, 6, pp. 63-71.

[47] Utami, S; Daud, A. Pengaruh Temperatur Panel Surya Terhadap Efisiensi Panel Surya. J. Tek. Energi, 2021, 11, pp. 7-10.

[48] Setiawan, M.T.; Winarno, I; Dewantara, B. Y. Implementasi Internet of Things Dalam Rancang Bangun Sistem Monitoring Pada Solar Cell Berbasis Web," JEECOM, 2021, 3, pp. 34-38,

[49] Cheragee, S.H; Hassan, N; Ahammed, S; Islam, A.Z.M.T. A Study of IoT Based Real-Time Solar Power Remote Monitoring System," IJASA, 2021, 9, pp. 27-36.

[50] Adanta, D; Syofii, I; Sari, D. P; Wiyono, A. Performance of Pico Scale Turgo Turbine in Difference the Nozzle Diameter. International Journal of Fluid Machinery and Systems, 2022, 15, pp. 130-136.

[51] Laudani, A; Lozito, G. M; Fulginei, F. R. Irradiance sensing through PV devices: A sensitivity analysis. Sensors, 2021, pp. 1-29.

[52] El-Hajj, M; Mousawi, H; Fadlallah, A. Analysis of Lightweight Cryptographic Algorithms on IoT Hardware Platform. Future Internet. 2023, pp. 1-29

[53] Liu, Y; Li, D; Du, B; Shu, L; Han, G. Rethinking sustainable sensing in agricultural Internet of Things: From power supply perspective. IEEE Wireless Communications, 2022, 29, pp. 102-109.

[54] Amanlou, S; Hasan, M. K; Bakar, K. A. A. Lightweight and secure authentication scheme for IoT network based on publish–subscribe fog computing model. J.Comnet, 2021, 199, pp. 1-22.

[55] Pahmi, M; Ayob, A; Ansari, S; Saad, M.A.M. Artificial Neural Network Based Forecasting of Power Under Real Time Monitoring Environment. IEEE SENNANO conference, 2021, p. 122-125.

[56] Aziz, L; Wahiddin, D and Lestari, S.A.P. Penerapan Dual Axis Solar Tracking dengan Fuzzy Logic Controller untuk Optimalisasi Output pada Solar Cell. Scientific Student Journal for Information, Technology and Science, 2021, 2, pp. 203-213.

[57] Manfaluthy, M; Pangestu, A; Arif, R; Sanjaya, L.A. Watt peak meter of solar panel," J. Phys.:Conference series, IOP Publishing Ltd, 2021, 1, pp. 1-12.

[58] Liu, H; Wu, R; Guo, Q; Hua, Z and Wu, Y. Electronic nose based on temperature modulation of MOS sensors for recognition of excessive methanol in liquors. ACS omega, 2021, 6, pp. 30598-30606.

[59] Smith, C; Satme, J; Martin, J; Downey, A. R. J; Vitzilaios, N; Imran, J. UAV rapidly-deployable stage sensor with electro-permanent magnet docking mechanism for flood monitoring in undersampled watersheds. Elsevier, 2022, 12, pp.1-19.

[60] Gupta, V.; Sharma, M.; Pachauri, R. K. & Babu, K. N. D. A Low-Cost Real-Time IOT Enabled Data Acquisition System for Monitoring of PV System. Energy Sources, Part A: Recovery, Utilization, and Environmental Effects, 2020, 43, pp. 1-16.